BB

FORSCHUNGSZENTRUM
ROSSENDORF e.V.

FZR

FZR-56
September 1994
Preprint

R. Kotte, B. Kämpfer, J. Mösner,
W. Neubert, D. Wohlfarth et al.
(FOPI Collaboration)

Interplay of Collective Flow Phenomena and Velocity Correlations of Intermediate-Mass Fragments in Collisions of Au + Au at E = 100 − 400A·MeV

Interplay of Collective Flow Phenomena and Velocity Correlations of Intermediate-Mass Fragments in Collisions of Au + Au at $E = 100 - 400A$·MeV

R. Kotte[1], B. Kämpfer[1,2], J. Mösner[1], W. Neubert[1], D. Wohlfarth[1], J.P. Alard[5], V. Amouroux[5], Z. Basrak[13], N. Bastid[5], I.M. Belayev[9], L. Berger[5], Th. Blaich[8], S. Boussange[5], A. Buta[3], R. Čaplar[13], C. Cerruti[11], N. Cindro[13], J.P. Coffin[11], R. Donà[14], P. Dupieux[5], J. Erö[4], Z.G. Fan[6], P. Fintz[11], Z. Fodor[4], L. Fraysse[5], R. Freifelder[6], S. Frolov[9], A. Gobbi[6], Y. Grigorian[10], G. Guillaume[11], N. Herrmann[7], K.D. Hildenbrand[6], S. Hölbling[13], O. Houari[11], M. Ibnouzahir[5], S.C. Jeong[6], F. Jundt[11], J. Kecskemeti[4], P. Koncz[4], Y. Korchagin[9], M. Krämer[6], C. Kuhn[11], I. Legrand[3], A. Lebedev[9], V. Manko[10], T. Matulewicz[12], G. Mgebrishvili[10], D. Moisa[3], G. Montarou[5], I. Montbel[5], D. Pelte[7], M. Petrovici[3], P. Pras[5], F. Rami[11], V. Ramillien[5], W. Reisdorf[6], A. Sadchikov[10], D. Schüll[6], Z. Seres[4], B. Sikora[12], V. Simion[3], S. Smolyankin[9], U. Sodan[6], K. Teh[6], R. Tezkratt[11], M. Trzaska[7], M.A. Vasiliev[10], P. Wagner[11], J.P. Wessels[6], T. Wienold[7], Z. Wilhelmi[12], and A.V. Zhilin[9]

(FOPI Collaboration)

[1] *Forschungszentrum Rossendorf, PF 510119, D-01314 Dresden, Germany*

[2] *Institut für Theoretische Physik, Technische Universität Dresden, Dresden, Germany*

[3] *Institute for Physics and Nuclear Engineering, Bucharest, Romania*

[4] *Central Research Institute for Physics, Budapest, Hungary*

[5] *Laboratoire de Physique Corpusculaire, Université Blaise Pascal, Clermont-Fd., France*

[6] *Gesellschaft für Schwerionenforschung, Darmstadt, Germany*

[7] *Physikalisches Institut der Universität Heidelberg, Heidelberg, Germany*

[8] *Universität Mainz, Mainz, Germany*

[9] *Institute for Experimental and Theoretical Physics, Moscow, Russia*

[10] *Kurchatov Institute for Atomic Energy, Moscow, Russia*

[11] *Centre de Recherches Nucléaires, Université Louis Pasteur, Strasbourg, France*

[12] *Institute of Experimental Physics, Warsaw University, Warsaw, Poland*

[13] *Rudjer Bošković Institute Zagreb, Zagreb, Croatia*

[14] *Instituto Nazionale di Fisica Nucleare, Legnaro, Italy*

(September 30, 1994)

Abstract

Velocity correlations of intermediate mass fragments (IMFs), produced in collisions of Au + Au at 100, 150, 250, and 400 A·MeV beam energy, are extracted from measurements with the FOPI (phase I) detector system at SIS in GSI Darmstadt. The IMF correlation functions of peripheral and semi-central events are found to be strongly affected by the collective sideward motion of nuclear matter. The sideflow causes an enhancement of correlations at small relative velocities. This enhancement results from the mixing of differently azimuthally oriented events; it vanishes if the events are rotated into a unique reaction plane. Selecting violent central collisions, the comparison of the data with a Coulomb dominated final-state interaction model points to a radius of the expanding and multifragmenting source of $R_s \simeq 13$ fm for 100 A·MeV which appears shrinking by 20% when increasing the projectile energy to 400 MeV per nucleon. The deduced source radii are found to depend on the radial explosion energy used in the model. The inclusion of such a collective expansion is necessary for a reasonable description of the experimental single-particle spectra of the IMFs. The unique Coulomb suppression of small relative IMF velocities, found for the given beam energy range, is attributed to rather constant averaged next-neighbour distances $\langle d_{IMF} \rangle = 8.6 \pm 0.2$ fm of the IMF charge centers within the source at break-up time.

PACS number(s): 25.70.Pq

I. INTRODUCTION

Multifragmentation with the disintegration into a substantial number of intermediate mass fragments (IMFs) with charges $Z \geq 3$ is a well confirmed decay channel of highly excited systems formed in violent nucleus-nucleus collisions [1–6]. Some details of the fragment formation process may be understood in the framework of statistical models [7–10], where the degree of clusterization in dependence on the internal excitation of the system can be investigated. On the other hand, complete dynamical models are more appropriate for the interpretation of collective flow phenomena and cluster production [11–14].

Recent investigations of such heavy systems as gold on gold at beam energies above the so-called balance energy of about 60 A·MeV [15,16] have shown that the IMFs, more sensitively than light charged particles, carry specific information on the collective sideward flow of nuclear matter at semi-central collisions [17–19] as well as on the expansion (or even explosion) of the system for more compact collisions [20–22]. Since collective flow is preferentially visible in the IMF momentum space distributions this finding can be established by studying single-particle observables and their dependences on the nuclear charge or mass under exclusive conditions.

Two-particle IMF observables are of decisive importance for the understanding of not only the collision dynamics in momentum space, but also for the space-time extent of the disassembling excited nuclear matter. IMFs mainly experience repulsive final state Coulomb interaction, which prevents the proximity of such particles in momentum space. This has important consequences for relative-velocity and relative-angle correlation functions. The study of the degree of suppression of small relative velocities or relative angles delivers information about the space-time structure of the source which emits the reaction products.

At beam energies well below 100 MeV per nucleon such investigations point to source life times in the order of some hundred fm/c [23–26] which is suggested to be an indication of a sequential decay of a compound-nucleus like system. The dominance of a more instantaneous multifragmentation process is predicted by theoretical models in reactions of heavy nuclei at energies $E \simeq 100A$·MeV [7,8]. Indeed, in recent measurements of central collisions of the system Ar + Au a systematic decrease of the multifragmentation time scale from about 100 fm/c to 50 fm/c is found if the beam energy is increased from 35 to 110 A·MeV [27]. Multifragment emission time scales of $\lesssim$ 100 fm/c are also found in Xe (50A·MeV) + ^{nat}Cu and in Kr ($35 - 75A$·MeV) + Nb collisions, respectively [28,29]. For central Au + Au collisions at beam energies $E \geq 150A$·MeV the typical time scale of the particle emission from an expanding and multifragmenting source is estimated to be less than 30 fm/c [30]. It is obvious that the multifragmentation process can be considered as nearly instantaneous on the scale of the typical Coulomb interaction time of the fragments $\tau_{Coul} \simeq 10^{-21}$sec = 300 fm/c [31]. Thus, the problem of disentangling time scales vs. spatial source scales, which needs to be tackled in reactions at lower beam energies, tends to become less significant in central collisions at higher bombarding energies. At high excitation energy this is demonstrated recently in the reaction α (3.6A·GeV) + Au [32].

Two-body observables are sensitive to collective modes. In ref. [33] the authors study the influence of rotational collective motion and sideward flow onto azimuthal angle correlation functions measured for the system Ar+Sc at $35-110A$·MeV beam energy. It is suggested that multifragment azimuthal correlations carry some information on the intermediate-energy

reaction dynamics.

The influence of the transversal collective motion on correlation functions as well as the sensitivity of the freeze-out radius information to the radial expansion have been investigated in ref. [34], where for the first time IMF-IMF relative velocity and azimuthal relative-angle correlations are studied for central collisions of such a heavy system as Au + Au at 150 A·MeV. Here, this investigation is continued in the sense of a systematic study of the excitation function of two-particle IMF-IMF observables over the projectile energy range $100 - 400A$·MeV. We present experimental two-particle yields and correlation functions of collisions selected according to their centrality which are compared with a N-body Coulomb trajectory model incorporating necessary details of the expansion scenario. We also attempt to extract non-spherical break-up geometries[1] by looking for directional effects, i.e. differences of the correlation functions parallel and transversal to the sideward flow direction.

Our paper is organized as follows. In Section II the experimental setup is shortly described. Section III presents the event classification which is used for appropriate impact parameter sampling. Section IV defines the construction of two-particle correlation functions which are the relevant observables discussed in the present work. In Section V we show the experimental results of IMF-IMF correlation functions for the system Au + Au at different beam energies and for various event samples. An interpretation of these results by utilizing N-body Coulomb trajectory calculations is presented in Section VI. The influence of azimuthal anisotropies is discussed in Section VII. Finally, the experimental results and their interpretations are summarized in Section VIII.

II. EXPERIMENTAL SETUP

The data are taken by the highly granular outer plastic wall in a phase I measurement of the 4π-detector system FOPI at the heavy ion synchrotron SIS at GSI Darmstadt [38]. The octogonally symmetric outer wall, which consists of 8 radial sectors, covers the polar angles 7^o to 30^o with 512 scintillator strips each of them providing an energy loss and time-of-flight signal. Low detection thresholds are achieved with the help of a shell of ionization chambers in front of the outer plastic wall which deliver additional energy loss informations. Element identification is possible for charges $Z \leq 15$ with typical detection thresholds of 15 (50) A·MeV for $Z = 1(15)$. A helium-filled bag reduces energy losses and interactions of reaction products on their way between target and wall. The measured velocities are corrected for the energy loss in different media passed by the particles, including the gold target itself,

---

[1]Recently, differences between longitudinal and transversal correlation functions have been observed not only for two-proton correlations in the reactions $^{36}Ar + ^{45}Sc$ at 80 A·MeV and $^{129}Xe + ^{27}Al$ at 31 A·MeV [35] but also for two-fragment correlations in the reaction ^{36}Ar + Au at 50 A·MeV [36] which seem to confirm the suggestions that two-body IMF observables may contain signatures of various break-up geometries (e.g. toroids or disk-shaped nuclear configurations) predicted in theoretical investigations of the multifragmentation at intermediate-energy heavy-ion collisions [37].

which had a thickness of 50 (100, 150, 200) μm corresponding to 0.25 (0.5, 0.75, 1.0) % interaction probability at 100 (150, 250, 400) A·MeV beam energy. Double counting of one and the same particle caused by the tiny geometrical overlap of two strips or a nuclear reaction of the fragment in the detector material is mainly excluded in off-line analysis. Typical relative-velocity resolutions of IMF pairs of $\sigma(|\vec{v}_1 - \vec{v}_2|) \leq 0.005$ c are estimated [34].

III. EVENT CLASSIFICATION

Events are classified by different binning procedures [4,39]. We can use the multiplicity of all charged particles PM seen in the outer plastic wall. Its distribution shows the typical flat plateau and a steep fall-off at higher multiplicities. It is divided into five bins PM1−PM5. The highest-multiplicity bin PM5 starts at half the plateau value corresponding to an integrated cross section of about 250 mb and impact parameters of $b/b_{max} \lesssim 0.2$ in sharp cut-off approximation. (For the maximum impact parameter of a Au + Au collision of two touching spheres one has $b_{max} \simeq 15$ fm.) The remaining multiplicity range is subdivided into four equally spaced intervals. (For the integrated (geometrical) cross sections of the multiplicity bins at various beam energies see ref. [40].) We exclusively analyse events which are preselected with the charged particle multiplicity gate PM3−PM5 ($b/b_{max} \lesssim 0.5$) in order to suppress non-target interactions which mainly contribute to the lower multiplicities.

The double selection of small values (typically $D < 0.15 - 0.25$, cf. ref. [19]) of the transverse momentum directivity $D = |\sum_i \vec{p}_{\perp i}| / \sum_i |\vec{p}_{\perp i}|$ (the sums run over all charged particles with polar angles $1^o < \theta_{lab} < 30^o$ detected in the forward hemisphere of the center-of-mass system [c.m.]) together with the high multiplicity cut PM5 can be used to select high-centrality events with large observed azimuthal symmetry, however, at the cost of a further reduction of the integrated cross section down to a value of about 50 mb.

Finally, the event-wise determined ratio of the sums of transverse and longitudinal c.m. kinetic energies $E_{rat} = \sum_i E_{\perp i} / \sum_i E_{\parallel i}$ is found to be a much more effective centrality measure (the sums run again over all charged particles with polar angles $1^o < \theta_{lab} < 30^o$ detected in the forward c.m. hemisphere) [19,39]. Already the single cut ERAT5 with about the same integrated cross section as in PM5 events (for 100, 150, 250, 400 A·MeV defined by $E_{rat} > 0.76$, 0.74, 0.72, 0.70, respectively) selects a pronounced IMF source at midrapidity, in a very similar way as the double cut PM5 & $D < 0.2$ does on a much less statistical level. Recently, most violent collisions with averaged impact parameters below 1.5 fm have been selected for 150 A·MeV applying the strong double event selection criterion $E_{rat} > 0.9$ & $D < 0.2$ [21]. The selection of such small impact parameters would be particularly interesting since recent calculations [41,42] performed within the BUU [43] and QMD approaches [12,13] predict in this region a transition of the momentum space configuration from prolate to oblate shapes. Experimental investigations applying new methods of event sampling in view of the isolation of those collisions with maximum stopping and preferential transverse expansion [14] are under consideration [44].

However, such high centrality cuts are for practical reasons of available statistics not useful in view of correlation analyses. Therefore, in the present paper, we restrict ourselves to ERAT5 events, i.e., to rather central collisions, for which typical averaged geometrical impact parameters of $\langle b \rangle \simeq 2.2$ fm are elucidated [4,40]. (For 150 A·MeV a slightly different

determination of the averaged impact parameter of the ERAT5 event class, $\langle b \rangle \simeq 2.5$ fm, is derived in ref. [21] where the E_{rat} distribution of impact parameter weighted QMD calculations [12] is investigated.) It is obvious that even in these rather central collisions residual azimuthal anisotropies resulting from the presence of a finite (about 50% of the maximum value [19,45]) sideward flow are present.

Further information on one-body observables and on various event characterizations can be found in refs. [4,19–21,39,40,45,46]. In Table I the number of events selected by the criteria PM3–PM5 and ERAT5 and the number of coincident IMF pairs contained in those event classes are summarized for the four projectile energies under consideration.

IV. THE CORRELATION FUNCTION

Let $Y_{12}(\vec{v}_1, \vec{v}_2)$ be the coincidence yield of IMF pairs with charges Z_1, Z_2 and velocities $\vec{v}_1$, $\vec{v}_2$. Then the two-particle correlation function is defined as [23]

$$1 + R(\vec{v}_1, \vec{v}_2) = \mathcal{N} \frac{\sum_{events,pairs} Y_{12}(\vec{v}_1, \vec{v}_2)}{\sum_{events,pairs} Y_{12,mix}(\vec{v}_1, \vec{v}_2)}. \tag{1}$$

The sum runs over all events and pairs fulfilling certain selection criteria (see chapter 3). Event mixing, denoted by the subscript "mix", means to take IMF #1 and IMF #2 out of different events. We only mix events found within the same event class. $\mathcal{N}$ is a normalization factor fixed by the requirement to have the same number of true and mixed pairs. The correlation function (1) is either projected onto the relative velocity

$$v_{12} = |\vec{v}_{12}| = |\vec{v}_1 - \vec{v}_2| \tag{2}$$

or onto the relative azimuthal angle in the plane perpendicular to the beam direction

$$\phi_{12} = |\phi_1 - \phi_2| = \cos^{-1}\left(\frac{\vec{v}_{\perp 1} \cdot \vec{v}_{\perp 2}}{v_{\perp 1} v_{\perp 2}}\right). \tag{3}$$

Besides the above mentioned global event characteristics we use gate conditions on the normalized rapidity $y^{(0)} \equiv (y/y_{proj})_{cm}$, or on the angle ξ between $\vec{v}_{12}$ and the pair velocity $\vec{V}_{12}^{cm} = \vec{v}_1^{cm} + \vec{v}_2^{cm}$.

Mutual Coulomb repulsion within an IMF pair is charge independent as long as the Coulomb repulsion energy dominates when using the scaled relative velocity $v_{red} \equiv v_{12}/\sqrt{Z_1 + Z_2}$ instead of the proper relative velocity v_{12}. Indeed, when displaying $1 + R$ vs. v_{red}, instead vs. v_{12}, we find that different charge combinations result in rather similar curves in the region of small relative velocities we focus on (see Fig. 1, discussion below). This scaling, predicted in ref. [47] and first verified experimentally in ref. [48], is used in the following. It allows for systematical studies of the correlation function even if rather restrictive event selection criteria are applied and provides the advantage of better statistics (cf. Table I) without loss of information.

The statistical errors of the correlation functions are governed by those of the coincidence yield, since the mixed yield is generated at least with an order of magnitude higher statistics.

V. RESULTS

A. Response of the apparatus

In order to study the influence of the experimental setup on the correlation function we have performed Monte Carlo simulations [49] with several event generators and the GEANT package [50]. As in the experimental data, we find an enhanced coincidence yield due to double counting at very small relative velocities ($v_{red} < 0.005$ c) mainly caused by scattering in the scintillator strips. This disturbing yield (about $0.3-1.1\%$ of the total relative-velocity yield of IMF pairs in PM3–PM5 events for $E = 100 - 400A$·MeV), which is stronger for peripheral collisions, is reduced drastically by excluding, around a given hit, positions on neighbouring strips within an azimuthal segment of $\Delta\phi = \pm(5^o - 7.5^o)$ for $100 - 400A$·MeV. (The same procedure is applied to the mixed yield.) This procedure excludes also true pairs. About $0.9 - 2.3\%$ of the IMF-IMF relative-velocity yield, depending on beam energy, are therefore rejected. However, the simulation allows us to determine a lower relative-velocity limit above which the experimental correlation function is not systematically affected: For instance, at 150 (250) A·MeV the correlation function after filtering by the response of the apparatus (the finite angular, velocity and charge resolutions, the energy thresholds and the exact geometry), suffers only minor distortions for relative velocities $v_{red}/c > 0.006$ (0.010).

B. Experimental data

In Fig. 1 the *Li-Be* and the *B-B* relative velocity correlation functions for IMF pairs from PM3–PM5 events are displayed. For $v_{red}/c < 0.03$ the correlation functions coincide within experimental accuracy. The right panel gives, as a function of $\sqrt{Z_1 + Z_2}$, the values of relative velocities v_{12} and v_{red} for which various IMF correlation functions ($Z_1 = Z_2 = 3$ to $Z_1 = 6$, $Z_2 = 7$) reach the value $R = -0.5$. A constant value of ~ 0.0134 c is observed if the data are plotted as function of the reduced velocity v_{red} (right panel, lower part). This allows for a suitable accumulation of all IMF pairs into a unique correlation function, whereas the IMF-IMF correlation function displayed as function of v_{12} would exhibit a rather large dispersion of the Coulomb flank, which shows up e.g. in the approximately linear increase of the $R = -0.5$ point vs. the square root of the charge sum (right panel, upper part).

In Fig. 2 the coincident yields of analysed pairs in ERAT5 events are displayed as function of the relative velocity for 150 and 400 A·MeV. The width of the relative velocity distributions is strongly biased by the detector acceptance. IMF-IMF relative-velocity distributions generated with a suitable model described below, exhibit up to 30% lower mean values of v_{red} after applying the detector filter with respect to the unfiltered ones. (This effect takes its maximum for lithium ions, i.e. the IMFs which are most extended in velocity space.) However, the low-velocity flanks of the correlation functions with and without filter are found to be nearly identical. This finding confirms the expectation that the influence of the detector acceptance vanishes in the small-relative velocity correlation function.

Fig. 3 displays, for different beam energies, the experimental correlation function of all IMF pairs in PM3–PM5 events. We find two different shapes of the correlation functions depending on the way of generating the uncorrelated (mixed) yield $Y_{12,mix}$. When using

the data directly, we find an enhancement of correlations for $v_{red} \sim 0.025$ c (open symbols). When rotating all events into a unique reaction plane (determined by the standard transverse momentum analysis [51], full symbols) before event mixing, this enhancement of correlations, arising from the contributions of differently azimuthally oriented events to the uncorrelated background $Y_{12,mix}$, vanishes. In this way we believe to eliminate widely the effect of the directed sideward flow. (Because of finite particle number effects the reaction plane determination is associated with a dispersion of typically $30^o - 40^o$ for PM4 events.) On the other hand, the enhancement could be used as a measure of the side flow [41]. It is, however, strongly biased by the detector acceptance.

Fig. 4 shows for 150 A·MeV beam energy the strong influence of the projectile bounce-off which is amplified with respect to the data displayed in Fig. 3 if one selects a sharp projectile rapidity gate $0.7 < y^{(0)} < 1.3$ on the IMFs in PM4 events (triangles). In case of discriminating against the influence of collective sideward motion by rotating the events into a unique reaction plane before mixing (full symbols) the Coulomb suppression appears stronger for central events selected by ERAT5 (dots). It is worthwhile noticing that no significant further shift of the correlation function is found if more restrictive E_{rat} conditions are applied or if approximately azimuthally symmetric PM5 & $D < 0.2$ or ERAT5 & $D < 0.2$ events are selected. (Of course, the event rotation does not make an effect if subgroups of azimuthally symmetric [i.e. low directivity] events are selected.) Pairs from the midrapidity region in PM5 events (squares) show the same correlation function as pairs from the ERAT5 events.

In Fig. 5 we compare for 150 A·MeV the ERAT5 correlation function (dots) with that of events with $0.41 < E_{rat} < 0.51$ (triangles), where the sideward flow has a maximum [19,21,45]; these event groups correspond to averaged impact parameters of $\langle b \rangle \simeq 4$ fm. The difference in the maximum of positive correlations at $v_{red} \sim 0.025$ c of Figs. 4 and 5 (open triangles in both figures), are attributed to the selection of a purer sample of well-aligned spectators when gating on projectile rapidities in PM4 events on the one side and to the bias of the detector acceptance which more seriously influences the region near midrapidity [4,19,21,38] on the other side.

Fig. 6 shows the experimental azimuthal relative-angle correlation functions of IMF pairs in the forward c.m. hemisphere for semi-central events (selection criterion PM3−PM5, left panel) and for central events (selected by the ERAT5 cut, right panel) at various beam energies. We find a suppression of correlations at small relative angles due to the mutual Coulomb forces which compete with positive correlations as consequence of the collective sideward motion of bouncing nuclear matter. When increasing the projectile energy, the influence of the collective motion increases, and the Coulomb hole becomes less obvious. Thus, the net correlation functions at 400 A·MeV show only a small residue of the Coulomb interaction. For the ERAT5 event selection, which still exhibits about 50% of the maximum sideward flow (cf. ref. [45]), this competition leads to a nearly flat curve.

In the following only those collisions are considered which may be described by a single central source (not necessarily spherically symmetric but at least located at midrapidity). Experimental two-dimensional distributions of the (Lorentz-invariant) cross section in the transverse momentum versus rapidity plane show such a single source behaviour if either the PM5 & $D < 0.2$ or the ERAT5 event selection criteria are applied to the FOPI data [19,21,39]. Moreover, previous BUU calculations [41] predict a continous transition from a

one-source to a two-source behaviour in the range of impact parameters of $b = 3 - 6$ fm. Therefore, we believe that events, selected by the ERAT5 criterion, which give still sufficient statistics for performing IMF-IMF correlation analysis (cf. Table I), are well suited to be described within a single source model (see chapter 6).

Fig. 7 shows the relative-velocity correlation function for ERAT5 events at various beam energies. In case of event rotation into a unique reaction plane (right panel) the correlation function shows a steeper slope for the lower projectile energies and a flatter one for the higher ones. Without regard of the reaction plane (left panel) we find a reverse trend: The Coulomb hole seems to fill up more for the higher beam energies due to the residual influence of the collective sideward motion - an observation which is much more apparent in Figs. 3 and 6.

Finally, longitudinal and transversal correlation functions (i.e., pairs with $\xi = 0°-30°$ / $150°-180°$ and $\xi = 70°-110°$) of events selected either by the PM3−PM5 or by the ERAT5 criterion show strong splittings (comparable to those displayed in Figs. 3 and 4) which, however, vanish when rotating all events into a unique reaction plane.

VI. INTERPRETATIONS

In order to understand these experimental results and their global dependences we have performed simulations, the results of which have been passed through the detector filter. In the following we show that for central events (characterized here by ERAT5) the parameters of the simulation are widely constrained by single-particle experimental data.

A. The Coulomb explosion model

The present interpretation is based on Monte Carlo calculations using a N-body Coulomb trajectory model [34,52]. At the beginning it generates charged clusters with a given charge distribution dN/dZ with $\sum_i Z_i = 2Z_{Au}$, which are randomly distributed in a suitable source volume (see below) avoiding overlaps within a sphere of radius $1.2A^{1/3}$ fm. We use $A = 2Z$ which is well founded by the experiment: Recently, isotopic ratios of light charged particles produced in central Au + Au collisions selected by the ERAT5 condition have been determined [53]. The averaged mass-to-charge ratio of $Z = 1$ particles, which is expected to exhibit the strongest deviation from the ratio 2, is $\langle A/Z \rangle = 1.89$ (1.90, 1.88) for 100 (150, 250) A·MeV projectile energy. The IMF charge distribution in the present experiments is found to fall off exponentially like $dN/dZ \sim A_Z \cdot e^{-\alpha Z}$ ($A_Z = 1$ for $Z \geq 3$) for central events [46]. The slope parameter α and the averaged multiplicities $\langle PM \rangle$ and $\langle M_{IMF} \rangle$ of charged particles and IMFs, respectively, detected in the outer wall are used to fix the input charge and multiplicity distributions. The yields of Z =1, 2 particles, which do not follow exactly the exponential behaviour, are scaled-up with suitable factors $A_1 \simeq 3$, $A_2 \simeq 2$ which are adjusted so that the corresponding particle multiplicities reproduce the experimental ones after applying the experimental filter. A homogeneous density distribution of the source is reached by putting the particles into the volume successively with decreasing charge.

Initially, the particles have a Maxwellian velocity distribution characterized by a temperature parameter T.

We distinguish a simple spherical model and an anisotropic model. Our main results are interpreted within the spherical model: The source volume is a sphere of radius R_s. A collective radial expansion, with linear velocity profile

$$\vec{v}(\vec{r}) = (\vec{r}/R_s)v_{surf} \tag{4}$$

(with v_{surf} as adjustable parameter), is superimposed on the random thermal initial motion. The velocity of the radial expansion profile is related to a mean flow energy by

$$\langle E/A \rangle_{flow} = \frac{m_N}{2}\frac{3}{5}v_{surf}^2 \tag{5}$$

with m_N being the nucleon mass. After Coulomb evolution the particle ensemble is Lorentz boosted in longitudinal direction to account for the c.m. motion. Typically, $5 \cdot 10^4$ events corresponding to some 10^5 IMF pairs within the outer wall acceptance have been generated for each parameter set (cf. Table I for the experimental statistics).

The temperature parameter is determined by energy conservation:

$$E_{cm} = E_{bind} + E_{therm} + E_{flow} + E_{Coul}. \tag{6}$$

For instance, at 150 A·MeV projectile energy the available c.m. energy of $(E/A)_{cm} \simeq 37$ MeV is assumed to share into averaged binding energy of $\langle E/A \rangle_{bind} \simeq 4 - 5$ MeV, initial radial explosion energy of $\langle E/A \rangle_{flow} = 12$ MeV, Coulomb expansion energy of $\langle E/A \rangle_{Coul} \simeq 4 - 5$ MeV, and the remaining energy of the random thermal motion. The latter thermal energy $\langle E/A \rangle_{therm} = \frac{3}{2}\frac{T}{<A>}$ together with the averaged mass number (including the neutrons) $\langle A \rangle = 2.2$ determines the value of the temperature parameter to $T = 25$ MeV as given in Table II. (The mean collective radial flow energy $\langle E/A \rangle_{flow}$ of Table II only contains the contribution from the self-similar expansion profile (4) and not the additional energy contribution from the Coulomb expansion.) So we have essentially two free parameters, $\langle E/A \rangle_{flow}$ and R_s. The former one we fix by reproducing the experimental single-particle energy spectra, the latter one by fitting the two-particle correlation function. The reproduction of the single particle distributions is a fundamental prerequisite for a reliable interpretation of the correlation functions.

B. Comparison with single-particle data

Fig. 8 compares the dependence of the experimental averaged kinetic energies per nucleon on the charge number Z with the corresponding results of Coulomb simulations using the input parameters of Table II with (full line) and without (dashed line) radial expansion. The kinetic energies are integrated over the c.m. polar angle range $25° < \Theta_{CM} < 45°$ which is essentially unbiased by the detector cuts. Applying an additional low-directivity cut $D < 0.2$, which singles out highly azimuthally symmetric events, does not change the mean kinetic energies by more than 5%. Thus, the full azimuthal integration of the slightly anisotropic ERAT5 events gives practically the same result as for azimuthally isotropic subevents.

Fig. 9 displays the corresponding IMF kinetic energy distributions. Also for the other beam energies we do well reproduce the experimental single particle spectra with the parameters of Table II. Without flow it is impossible to describe the mean values and the shape of the spectra (cf. Figs. 8 and 9 and refs. [20–22]). Also a reasonable variation of the radius parameter R_s does not change the single-particle spectra significantly. With the energy parameters fixed in this way also the experimental relative-velocity distributions of different IMF combinations, displayed in Fig. 2, are well reproduced.

C. Comparison with two-body data

Before comparing with the experimental correlation functions we consider the behaviour of the simulated correlation function with respect to the charge scaling. We find a good reproduction of the scaling with v_{red} within our N-body Coulomb trajectory calculations. (Not displayed since when plotting the correlation functions of different IMF charge combinations the curves lie indeed on top of each other.) This observation is somewhat unexpected (but in line with the experimental data displayed in Fig. 1) since the scaling was originally predicted for dominating two-body Coulomb interaction [47].

Fig. 10 demonstrates the importance of the radial expansion. Without flow the simulated correlation functions would fit the experimental ones only if one introduces stronger Coulomb suppressions by using source radii which are much smaller (about a factor of 2 !) than the optimum ones given in Table III. Thus, the radial explosion increases the width of the Coulomb hole at small relative velocities (while the random thermal motion acts oppositely). The flow is, however, uniquely determined by the above single-particle observables. It is worth noticing that the radial flow causes a correlation of configuration space and momentum space distributions.

We have studied the sensitivity of the results on the temperature parameter: A change of the random thermal motion leads only to minor distortions of the correlation function even when varying the temperature parameter T by a factor of two [34,52]. This is due to the fact that the energy distributions of the IMFs are mainly governed by the radial explosion component whereas the thermal part decreases with $1/A$ (cf. Figs. 8 and 9).

In Fig. 11 the results of simulations using the parameters of Table II but three different source radii (R_s = 10, 16, 30 fm) are overlayed onto the experimental correlation functions of IMF pairs from ERAT5 events for the projectile energies $E = 100 - 400A$·MeV (cf. right panel of Fig. 6). With increasing beam energy the separation of the curves R_s = 10 fm and R_s = 30 fm increases. In order to find the optimum source radius (which is the only remaining free parameter for fitting the Coulomb flank of the correlation function) we perform χ^2 minimizations of the simulated correlation functions with respect to the experimental data for IMF pairs from central (ERAT5) events. For the optimum values of R_s our model describes the experimental date very well. We find $R_s \sim 13$ fm at 100 A·MeV and a slight shrinking of about 20% of the source radius when going to 400 A·MeV beam energy. The optimum source radii are given in Table III.

D. Discussion

Recently, correlation functions involving light composite particles (mainly α particles) have been studied also for ERAT5 selected central collisions of Au + Au at 150 and 400 A·MeV in ref. [54]. The observed correlation functions exhibit resonance structures arising from excited states of heavier fragments. The comparison of the experimental correlation functions with theoretical ones, calculated for Gaussian sources $\rho(r) = \rho_0 \cdot exp(-r^2/R_G^2)$ with negligible life times [55] give very similar results as reported in the present IMF-IMF correlation analysis. The transformation of the fitted Gaussian source radii R_G to sharp sphere radii using $R_s = (5/2)^{1/2} R_G$ (which can be justified by equating the rms radii of the two density distributions) results in the values of $R_s = 13.5 \pm 0.8$ (11.1 ± 0.8) fm which have to be compared with the data of 150 (400) A·MeV projectile energy given in Table III. These are negligible differences in the absolute values, and the common finding of these two methodically independent investigations is the reduction of the source radius of central collisions when increasing the projectile energy.

Within the Coulomb trajectory code it is possible to calculate also the next-neighbour distances of the IMF charge centers within the source at freeze-out. This can be done directly, thus avoiding the approximation $d_{IMF} = 1/\rho_{IMF}^{1/3} = (\text{volume}/\langle M_{IMF} \rangle)^{1/3}$ which holds for large particle numbers only. The corresponding values $\langle d_{IMF} \rangle$ (averaged over the event ensemble) are given in the right column of Table III. We find a rather constant value of $\langle d_{IMF} \rangle = 8.6 \pm 0.2$ fm over the whole projectile energy range. This interesting finding is understandable if one simultaneously considers the optimum source radius and the mean IMF number in the source (the latter number is determined before filtering the simulation results as about 14, 10, 8 and 5 for 100, 150, 250 and 400 A·MeV beam energy, respectively) since both quantities decrease for increasing beam energy (Table III, cf. also ref. [5]). Following ref. [34] the initial relative distance given above can be transformed to a scaled relative velocity $\langle v_{red} \rangle = (\frac{e^2}{m_N \langle d_{IMF} \rangle})^{1/2} = 0.0134$ c (e stands for the elementary charge). This number compares well with the 50% crossing point of the correlation function given in Fig. 1 (right panel).

We have investigated also the influence of the number of charged particles contained in the source. There is only a very slight change of the IMF-IMF correlation function if - in the extreme case - the particle number is restricted to the IMFs alone and the light species are completely taken out. Thus, the surrounding charge cloud of the light charged particles does not significantly disturb the mutual Coulomb interaction of the IMFs whose distance is responsible for the almost constant Coulomb hole in the relative-velocity correlation function at different beam energies. This result is in agreement with findings of ref. [41] where for 150 A·MeV the authors, within a hybrid model, take over only $50-75\%$ of the total nucleon number from the BUU approach to the Copenhagen Statistical Multifragmentation Model [8] which is able to generate and deexcite composite particles and follow their Coulomb trajectories.

For 150 A·MeV also the expansion of a spherical shell (outer radius R_s =16 fm and the same volume and the same input parameters as given in Table II for the sphere) is studied. The correlation function shows only minor differences with respect to our standard model of the radially exploding sphere. Since for the spherical shell with spherical initial explosion

pattern the kinetic energy distributions are nearly the same as for the spherical expansion curves (full lines) given in Fig. 9 (except of a yield suppression for heavier clusters with charges $Z \geq 5$ at very small energies $E_{cm}/m_0c^2 < 0.1$) one would expect the same also for the correlation function. This observation supports the demand of a careful description of the experimental single particle spectra before studying the two-particle observables.

VII. DISCUSSION OF ANISOTROPIES

The previous discussion applies for the set of azimuthally isotropic events as selected by the PM5 & $D < 0.2$ or ERAT5 & $D < 0.2$ criteria. However, since the ERAT5 event class shows a non-vanishing azimuthal anisotropy (cf. Figs. 6 and 7) arising from the sideward flow it is worth showing that a model relying on an anisotropic source with anisotropic expansion pattern does not change the above results significantly within present accuracy. For 150 A·MeV we run the anisotropic model with the same parameters as given in Table II for the isotropic model but modelling the source in the following way.

Now the source volume is a cylinder of radius $R_\perp$ and length $2L$. We set $R_\perp = L = 10$ fm which gives the same averaged IMF next-neighbour distance and nearly the same volume as a sphere with the optimum radius $R_s = 12$ fm given in Table III. Initially, an anisotropic linear expansion profile

$$\vec{v}(\vec{r}) = (\vec{r}_\perp/R_\perp)v_{\perp surf} + (\vec{r}_{||}/L)v_{||surf} \tag{7}$$

is superimposed on the random thermal initial motion. The mean flow energy (here divided into the eigenvalues which apply to the local coordinate system of the cylinder)

$$\langle E/A\rangle^{flow}_{x,y,z} = \frac{m_N}{2}(\frac{1}{4}v^2_{\perp surf}\ ,\ \frac{1}{4}v^2_{\perp surf}\ ,\ \frac{1}{3}v^2_{||surf}) \tag{8}$$

with $\langle E/A\rangle^{flow}_{x,y,z} = (2,2,8)$ MeV gives the same total energy residing in the system as for the spherical case (cf. Table II). Then the expanding source is tilted by the flow angle $\Theta_{flow} = 50^o$ (the angle between the source symmetry axis and the beam direction). The reaction plane is randomized afterwards. Flow values similar to ours have been predicted independently within a BUU approach for the impact parameter range under consideration [41]. However, the rather large flow angle (compared with typically 30^o to 40^o determined in the LBL/GSI plastic ball experiments [56] and also within BUU calculations [41,57]) is supposed to be a consequence of the specific bias of the ERAT5 event selection criterion which - together with the FOPI stage I acceptance - may favour such prolate event configurations which are more rotated off the beam axis[2]. Note also that the present source parametrization applies prior to Coulomb evolution which tends to cause more isotropy in the final state. Thus our modelling should be understood as an explorative case to study

---

[2]Recently, similar large flow angles have been predicted within transport model simulations [58] for the system Au + Au at 400 A·MeV when selecting impact parameters of $b/b_{max} < 0.2$.

the effect of anisotropies on two-body observables. Our parameters are fixed by comparing the simulation output with various experimental findings.

In Fig. 12 the distribution of the IMF azimuthal angles relative to the reaction plane (left panel) and the azimuthal relative-angle correlation function (right panel) of IMF pairs are given for the forward c.m. hemisphere at 150 A·MeV Au + Au. A rather perfect agreement of the simulation results with the experimental data is obtained for these two azimuthal observables.

Fig. 13 shows the relative-velocity IMF correlation function at $E = 150A$·MeV with and without the rotation of the events into a unique reaction plane before mixing. Indeed, a perfect description of both correlation functions is possible with the parameters of the anisotropic model given above.

Fig. 14 displays, analogously to Fig. 8, the dependence of the mean kinetic energy per nucleon $\langle E/A \rangle$ vs. the fragment charge Z now for three bins of the azimuthal angle relative to the reaction plane $|\phi - \phi_{rp}|$ (cf. Fig. 12, left panel). A quite good reproduction of the experimental behaviour is achieved. These findings show that the essential anisotropies are correctly uncovered by such a model.

Using this anisotropic model we try to find out whether one can determine the different spatial source extensions of non-spherical break-up configurations when viewing the expanding source from different orientations (cf. ref. [35,37]). For this goal we model the source as a strongly elongated cylinder also in coordinate space ($R_\perp = 8.3$ fm, $L = 16.6$ fm with the same volume as a sphere of radius R_s =12 fm) and the anisotropic flow given above. When dividing the IMF azimuthal angle relative to the reaction plane (cf. Fig. 12, left panel) into three bins (each 60° wide; in the present investigation, smaller bins are not suitable due to statistical reasons) we generate different correlation functions (both for the experimental data of ERAT5 events and the Coulomb trajectory simulations). Taking into account the bias of the detector acceptance, the correlation function of IMF pairs emitted into the main flow direction should be sensitive to the long shaped axis of the source; the correlation function of pairs from the opposite side would measure the smaller extension.

However, no relevant differences have been observed neither in experiment nor in simulations when viewing the source from different orientations relative to the reaction plane (a finding which is also supported by the observation of no differences between longitudinal and transversal correlation functions). Either this means that the binning is too coarse, or the Coulomb dominated correlation function is hardly sensitive within present statistics to the real source extension but predominantly to the inter-particle distance. The latter explanation is supported by the observation of constant next-neighbour distances of the IMFs within the multifragmenting spherical source at break-up time (see above).

Though the reproduction of the selected experimental observables with the anisotropic flow model seems to be almost perfect it should be considered as an extreme example rather than a final fit of flow patterns since a part of the phase space is not covered by the detector.

VIII. SUMMARY

In summary we present small-angle and small-relative-velocity correlations of IMFs produced in central collisions of Au + Au at $100 - 400A$·MeV. The data are compatible with

a fast (instantaneous) multifragmentation picture of a radially expanding source created in central collisions.

The importance of both radial explosion and collective sideward motion of nuclear matter for the data interpretation is shown. Whereas the influence of the in-plane flow can be eliminated by rotating the events into a unique reaction plane, the radial expansion of compressed nuclear matter found for violent collisions above 100 A·MeV projectile energy has to be taken into consideration in models dedicated to the determination of the source extension at break-up time. The flow decisively affects the output of optimization procedures (i.e. the source radius).

Taken into account the radial flow energies, which essentially govern the IMF kinetic energy spectra, the comparison of IMF relative-velocity correlation functions generated with a Coulomb dominated final state interaction model delivers a source radius which amounts to 13 fm for 100 A·MeV beam energy and shrinks by about 20% for 400 A·MeV. However, the averaged distance between the IMF charge centers in the source at break-up time is found to be nearly constant ($\langle d_{IMF} \rangle = 8.6 \pm 0.2$ fm) over the entire projectile energy range.

In any case, our data interpretation indicate a strong expansion effect. The extracted source radii are larger than a $2A_{Au}$ system at nuclear saturation density. The slight reduction of the source extension with increasing beam energy is in line with the results of various heavy-ion reactions at projectile energies below 100 A·MeV, where a reduction of the space-time extent with increasing energy has been found. The almost unique Coulomb suppression at small relative velocities of the correlation function found over the entire projectile energy range studied supports the suggestion that the Coulomb dominated IMF-IMF correlation functions are less sensitive to the source extension but to the distances between the IMFs within the source, which easily can be handled within the framework of the present model.

Further detailed investigations of different geometrical freeze-out shapes, directional effects and flow patterns as well as higher order reduced-velocity correlation functions (a new technique which is proposed to carry enhanced signatures of the reaction dynamics of multifragmentation [59]) are under consideration.

Acknowledgements. We are grateful for many discussions to H.W. Barz, C.K. Gelbke, D.H.E. Gross, J. Pochodzalla and W. Trautmann. This work is supported by means of BMFT under contracts No. 06 DR 105 and No. 06 DR 107.

REFERENCES

[1] K.G.R. Doss et al., Phys. Rev. Lett. **59**, 2720 (1987)
[2] C.A. Ogilvie et al., Phys. Rev. Lett. **67**, 1214 (1991)
[3] J. Hubele et al., Z. Phys. **A340**, 263 (1991)
[4] J.P. Alard et al., Phys. Rev. Lett. **69**, 889 (1992)
[5] M.B. Tsang et al., Phys. Rev. Lett. **71**, 1502 (1993)
[6] G.F. Peaslee et al., Phys. Rev. C **49**, R2271 (1994)
[7] D.H.E. Gross, Z. Phys. **A309**, 41 (1982), Phys. Rev. Lett. **68**, 146 (1986), Rep. Progr. Phys. **53**, 605 (1991), Nucl. Phys. **A553**, 175c (1993)
[8] J.P. Bondorf, R. Donangelo, I.N. Mishustin, and H. Schulz, Nucl. Phys. **A444**, 460 (1985),
J.P. Bondorf, R. Donangelo, H. Schulz, and K. Sneppen, Phys. Lett. **162B**, 30 (1985)
[9] H.W. Barz, J.P. Bondorf, K. Sneppen, and H. Schulz, Phys. Lett. **244B**, 161 (1990)
[10] W.A. Friedman, Phys. Rev. C **42**, 667 (1990)
[11] G. Peilert, H. Stöcker, W. Greiner, A. Rosenhauer, A. Bohnet, and J. Aichelin, Phys. Rev. C **39**, 39 (1989),
G. Peilert et al., Phys. Rev. C **46**, 1457 (1992)
[12] A. Bohnet, J. Aichelin, J. Pochodzalla, W. Trautmann, G. Peilert, H. Stöcker, and W. Greiner, Phys. Rev. C **44**, 2111 (1991)
[13] J. Aichelin, Phys. Rep. **202**, 233 (1991)
[14] P. Danielewicz and Q. Pan, Phys. Rev. C **46**, 2002 (1992)
[15] G.D. Westfall et al., Phys. Rev. Lett. **71**, 1986 (1993)
[16] S. Soff, St. A. Bass, C. Hartnack, H. Stöcker, and W. Greiner, GSI Darmstadt Scientific Report 1993, GSI-94-1, p. 84 (1994)
[17] H.H. Gutbrod, A.M. Poskanzer, and H.G. Ritter, Rep. Progr. Phys. **52**, 1267 (1989), H.H. Gutbrod et al., Phys. Lett. **216B**, 267 (1989), Phys. Rev. C **42**, 640 (1990)
[18] S. Costa et al., Proc. XXXII Int. Wintermeeting on Nucl. Phys., Bormio, Italy 1994
[19] N. Herrmann, Nucl. Phys. **A553**, 739c (1993)
[20] W. Reisdorf, Acta Physica Polonica **B25**, 433 (1994), Proc. of the XXII Int. Workshop on Gross Properties of Nuclei and Nuclear Excitations, Hirschegg, Austria 1994, p. 93, (ed. H. Feldmeier, GSI Darmstadt)
[21] S.C. Jeong et al., Phys. Rev. Lett. **72**, 3468 (1994)
[22] W.C. Hsi et al., MSU preprint, MSUCL-930 (1994)
[23] D.H. Boal, C.K. Gelbke, and B.K. Jennings, Rev. Mod. Phys. **62**, 553 (1990)
[24] Z. Chen et al., Phys. Rev. C **36**, 2297 (1987),
Y.D. Kim et al., Phys. Rev. Lett. **67**, 14 (1991)
[25] R. Trockel et al., Phys. Rev. Lett. **59**, 2844 (1987)
[26] T.C. Sangster, M. Begemann-Blaich, T. Blaich, H.C. Britt, A. Elmaani, N.N. Ajitanand, and M.N. Namboodiri, Phys. Rev. C **47**, R2457 (1993)
[27] D. Fox et al., Phys. Rev. C **47**, R421 (1993)
[28] D.R. Bowman et al., Phys. Rev. Lett. **70**, 3534 (1993)
[29] E. Bauge et al., Phys. Rev. Lett. **70**, 3705 (1993)
[30] B. Kämpfer, R. Kotte, J. Mösner, W. Neubert, and D. Wohlfarth, FZ Rossendorf preprint, FZR 93-14 (1993)

[31] O. Schapiro and D.H.E. Gross, Nucl. Phys. **A573**, 143 (1994), ibid. **A576**, 428 (1994)
[32] V. Lips et al., Phys. Rev. Lett. **72**, 1604 (1994),
V. Lips et al., ibid., in press
[33] R.A. Lacey et al., Phys. Rev. Lett. **70**, 1224 (1993)
[34] B. Kämpfer et al., Phys. Rev. C **48**, R955 (1993)
[35] M.A. Lisa et al., Phys. Rev. Lett. **71**, 2863 (1993), Phys. Rev. C **49**, 2788 (1994)
[36] T. Glasmacher et al., Phys. Rev. C **50**, 952 (1994)
[37] T. Glasmacher, C.K. Gelbke, and S. Pratt, Phys. Lett. **314B**, 265 (1993),
C.K. Gelbke, invited talk at CORINNE 2, Nantes, France, Sept. 1994
[38] A. Gobbi et al., Nuclear Instruments and Methods in Physics Research **A324**, 156 (1993)
[39] W. Reisdorf, Proc. of the XX Int. Workshop on Gross Properties of Nuclei and Nuclear Excitations, Hirschegg, Austria 1992, p. 38, (ed. H. Feldmeier, GSI Darmstadt)
[40] Th. Wienold, Ph. D. thesis, GSI Darmstadt, Report GSI-93-28 (1993)
[41] B. Heide and H.W. Barz, FZ Rossendorf preprint, FZR-41 (1994), Phys. Lett. **B**, in press
[42] J. Konopka, H. Stöcker, and W. Greiner, Proc. of the XXII Int. Workshop on Gross Properties of Nuclei and Nuclear Excitations, Hirschegg, Austria 1994, p. 218, (ed. H. Feldmeier, GSI Darmstadt)
[43] G.F. Bertsch and S. Das Gupta, Phys. Rep. **160**, 189 (1988)
[44] J.P. Coffin, Contribution to the Taormina Conference, Italy, 1994, and to be published,
C. Kuhn, 7th Int. Conf. on Nucl. Reaction Mechanisms, Varenna, Italy, 1994,
J.P. Coffin, Proc. NASI on Hot and Dense Nuclear Matter, Bodrum, Turkey, 1993 (eds. W. Greiner and H. Stöcker, NATO ASI Series B, Plenum, N.Y., in press)
[45] Th. Wienold, Proc. NASI on Hot and Dense Nuclear Matter, Bodrum, Turkey, 1993 (eds. W. Greiner and H. Stöcker, NATO ASI Series B, Plenum, N.Y., in press)
[46] C. Kuhn et al., Phys. Rev. C **48**, 1232 (1993)
[47] Y.D. Kim, R.T. de Souza, C.K. Gelbke, W.G. Gong, and S. Pratt, Phys. Rev. C **45**, 387 (1992)
[48] Y.D. Kim, R.T. de Souza, D.R. Bowman, N. Carlin, C.K. Gelbke, W.G. Gong, W.G. Lynch, L. Phair, M.B. Tsang, and F. Zhu, Phys. Rev. C **45**, 338 (1992)
[49] R. Kotte, J. Mösner, W. Neubert, and D. Wohlfarth, FZ Rossendorf Annual Report 1992, FZR 93-10 (1993)
[50] R. Brun, F. Bruyant, M. Maire, A.C. McPherson, and P. Zanarini, GEANT3, CERN Data Handling Division, DD/EE/84-1, 10.1987
[51] P. Danielewicz and G. Odyniec, Phys. Lett. **157B**, 146 (1985)
[52] B. Kämpfer, R. Kotte, J. Mösner, W. Neubert, and D. Wohlfarth, Proc. of the XXII Int. Workshop on Gross Properties of Nuclei and Nuclear Excitations, Hirschegg, Austria 1994, p. 113, (ed. H. Feldmeier, GSI Darmstadt)
[53] M. Bini, P. Maurenzig, A. Olmi, G. Pasquali, G. Poggi, and N. Taccetti, Proc. NASI on Hot and Dense Nuclear Matter, Bodrum, Turkey, 1993 (eds. W. Greiner and H. Stöcker, NATO ASI Series B, Plenum, N.Y., in press)
[54] I. Montbel, Thesis, Univ. Blaise Pascal, Clermont-Fd., 1994, J.P. Alard et al., GSI Darmstadt Scientific Report 1993, GSI-94-1, p. 21 (1994)
[55] D.H. Boal, Ann. Rev. Nucl. Part. Sci. **37**, 1 (1987)

[56] K.-H. Kampert, J. Phys. G **15**, 691 (1989)
[57] H.W. Barz, private communication
[58] P. Danielewicz, MSU preprint, MSUCL-946 (1994)
[59] J. Lauret and R.A. Lacey, Phys. Lett. **327B**, 195 (1994)

TABLES

TABLE I. Number of events selected by the criteria PM3–PM5 and ERAT5 and number of coincident IMF pairs contained in those event classes for different projectile energies.

proj. energy E/A [MeV]	PM3–PM5 events	PM3–PM5 IMF pairs	ERAT5 events	ERAT5 IMF pairs
100	$1.2 \cdot 10^5$	$3.4 \cdot 10^5$	$0.8 \cdot 10^4$	$3.7 \cdot 10^4$
150	$2.7 \cdot 10^5$	$8.5 \cdot 10^5$	$1.5 \cdot 10^4$	$8.9 \cdot 10^4$
250	$1.7 \cdot 10^5$	$4.6 \cdot 10^5$	$1.8 \cdot 10^4$	$6.2 \cdot 10^4$
400	$1.8 \cdot 10^5$	$2.6 \cdot 10^5$	$1.5 \cdot 10^4$	$3.0 \cdot 10^4$

TABLE II. Input parameters of the Coulomb simulation code (spherical model).

projectile energy E/A [MeV]	charge distr. steepness α	temperature parameter T [MeV]	mean radial flow energy $\langle E/A \rangle_{flow}$ [MeV]
100	0.5	15	9
150	0.7	25	12
250	0.9	35	25
400	1.1	55	40

TABLE III. Source radii and next-neighbour IMF distances resulting from the fit of the correlation functions generated with Coulomb trajectory simulations (spherical model) to the corresponding experimental data.

projectile energy E/A [MeV]	sharp sphere radius R_s [fm]	next-neighbour IMF distance $\langle d_{IMF} \rangle$ [fm]
100	$13.3^{+0.8}_{-0.4}$	8.57 ± 0.3
150	$12.0^{+1.0}_{-0.5}$	8.55 ± 0.4
250	$11.0^{+1.6}_{-0.8}$	8.62 ± 0.6
400	$10.5^{+2.0}_{-1.0}$	8.63 ± 0.8

FIGURES

FIG. 1. The experimental relative-velocity correlation function as function of the reduced velocity v_{red} for two different IMF combinations from events characterized by the charged particle multiplicity bins PM3–PM5 (left panel). To minimize the influence of the directed sideward flow the events are rotated into a unique reaction plane before event mixing. Note that the mixed yield is correspondingly constructed either for charge combinations 3 - 4 or 5 - 5 from two events both carrying at least one such combination. The right panel displays, in dependence on $\sqrt{Z_1 + Z_2}$, the relative velocities v_{12} (upper part) and v_{red} (lower part) for which the IMF correlation functions of various IMF combinations ($Z_1 = Z_2 = 3$ to $Z_1 = 6$, $Z_2 = 7$) become $R = -0.5$. For better optical resolution, the data points of equal charge sums of the IMF pairs are slightly separated. The dashed lines are linear fits to the data in order to guide the eyes. Apparently, the correlation function vs. v_{red} in the region $1 + R < 0.8$ is independent of the charge combination.

FIG. 2. The coincidence yield Y_{12} at $E = 150A$·MeV (lower panel) and at $E = 400A$·MeV (upper panel) as function of the relative velocity for different IMF pair combinations Z_1 Z_2. Error bars: Experimental data of ERAT5 events (bin width 0.002 c, every fourth bin displayed only). Thin smooth lines: Results of the Coulomb simulation code using a radial expansion with the parameter set of Table II (normalized to the corresponding experimental yields). The overall agreement of simulations and experimental data for 100 and 250 A·MeV is similarly well.

FIG. 3. The experimental relative-velocity correlations of IMFs produced in semi-central collisions (selected by the PM3–PM5 cut) of Au + Au at various beam energies. Open symbols: without event rotation before mixing. Full symbols: with regard of the reaction plane, i.e. rotation into a unique reaction plane before event mixing.

FIG. 4. The experimental relative-velocity correlations of IMFs produced in collisions of Au + Au at 150 A·MeV for three different event characterizations. Triangles: IMF pairs from peripheral collisions characterized by the PM4 selection and an additional rapidity cut on the bounced projectile spectator $0.7 < y^{(0)} < 1.3$. Squares: IMF pairs from the midrapidity ($|y^{(0)}| < 0.4$) region of PM5 events. Dots: IMF pairs characterized by the central cut ERAT5 ($E_{rat} > 0.74$). The full (open) symbols give the correlation function with (without) taking into account the reaction plane.

FIG. 5. The experimental relative-velocity correlations of IMFs produced in collisions of Au + Au at 150 A·MeV for two different E_{rat} event characterizations. The triangles represent IMF pairs from semi-central collisions characterized by a gate on the E_{rat}-scale where the sideward flow has a maximum ($0.41 < E_{rat} < 0.51$) whereas the dots stand for IMF pairs characterized by the central cut ERAT5 ($E_{rat} > 0.74$). The full (open) symbols give the correlation function with (without) taken into account the reaction plane.

FIG. 6. The experimental azimuthal relative-angle correlation functions of IMF pairs in the forward c.m. hemisphere at various beam energies. Left panel: semi-central events (PM3–PM5). Right panel: central events (ERAT5).

FIG. 7. The relative-velocity correlation function for ERAT5 events at various beam energies. Right panel: The events are rotated into a unique reaction plane before mixing. Left panel: without event rotation before mixing.

FIG. 8. The mean kinetic energies per nucleon for various clusters. Squares: experimental data from ERAT5 events integrated over the full azimuthal angle and over the c.m. polar angle range $25^\circ < \Theta_{CM} < 45^\circ$. Curves: Coulomb simulation results (filtered through the same phase space region) using the parameters of Table II with (full line) and without (dashed line) radial expansion. The lines are fits $(p_1/Z + p_2)$ to the simulation results.

FIG. 9. Experimental invariant kinetic energy distributions ($d^2M/pdEd\Omega$, normalized by the number of events, integrated over the full azimuthal angle and over the c.m. polar angle range $25^\circ < \Theta_{cm} < 45^\circ$) of IMFs with $Z = 3 - 6$ from central Au + Au collisions at 150 A·MeV characterized by the ERAT5 event selection (dots) compared to the results of Coulomb trajectory simulations using the corresponding parameters given in Table II with (full lines) and without (dashed lines) radial expansion.

FIG. 10. The relative-velocity correlation function at $E = 150A$·MeV for IMF pairs from ERAT5 events (dots). The events are rotated into a unique reaction plane before mixing. The full (dashed) line corresponds to simulations using the corresponding parameters of Table II with (without) taken into account the radial expansion.

FIG. 11. The relative-velocity correlation function of IMF pairs from ERAT5 events (dots) of the reaction Au + Au at various beam energies. The events are rotated into a unique reaction plane before mixing. The full, dashed and dotted lines correspond to simulations using the parameters of Table II, but the radius parameters $R_s = 10$, 16, and 30 fm, respectively.

FIG. 12. Experimental IMF distribution of the azimuthal angle relative to the reaction plane (left panel, no exclusion of auto-correlations) and experimental azimuthal relative-angle correlation function (right panel) of IMF pairs in ERAT5 events in the forward c.m. hemisphere for 150 A·MeV Au + Au (full dots). The open squares give the corresponding result of a Coulomb simulation using an anisotropically expanding flow ellipsoid $\langle E/A\rangle_{x,y,z}^{flow} = (2, 2, 8)$ MeV tilted by a flow angle $\theta_{flow} = 50^\circ$ and the remaining parameters of Table II.

FIG. 13. The relative-velocity correlation function at $E = 150A$·MeV for IMF pairs from ERAT5 events. The dots (squares) give the resulting correlation function if the events are (are not) rotated into a unique reaction plane before mixing. The full and dashed lines are the corresponding results of a Coulomb simulation using an anisotropically expanding flow ellipsoid $\langle E/A \rangle_{x,y,z}^{flow} = (2, 2, 8)$ MeV tilted by a flow angle $\theta_{flow} = 50^o$ and the remaining parameters of Table II.

FIG. 14. The mean kinetic energies per nucleon for various clusters and three bins of the azimuthal angle relative to the reaction plane $|\phi - \phi_{rp}|$ (cf. Fig. 12, left panel). Full symbols: experimental data from ERAT5 events integrated over the c.m. polar angle range $25^o < \Theta_{CM} < 45^o$. Curves: Coulomb simulation results (filtered through the same phase space region) using the anisotropic model. The lines are fits $(C_1/Z + C_2)$ to the simulation results.

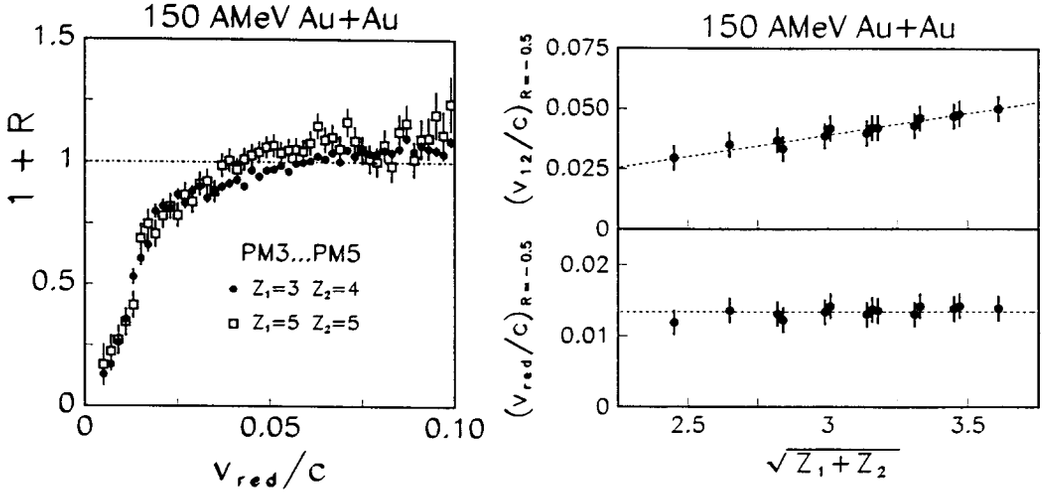
150 AMeV Au+Au
1 + R
PM3...PM5
Z₁=3 Z₂=4
Z₁=5 Z₂=5
v_red/c
150 AMeV Au+Au
(v_1,2/c)_R=-0.5
(v_red/c)_R=-0.5
√Z₁+Z₂

FIG. 1.

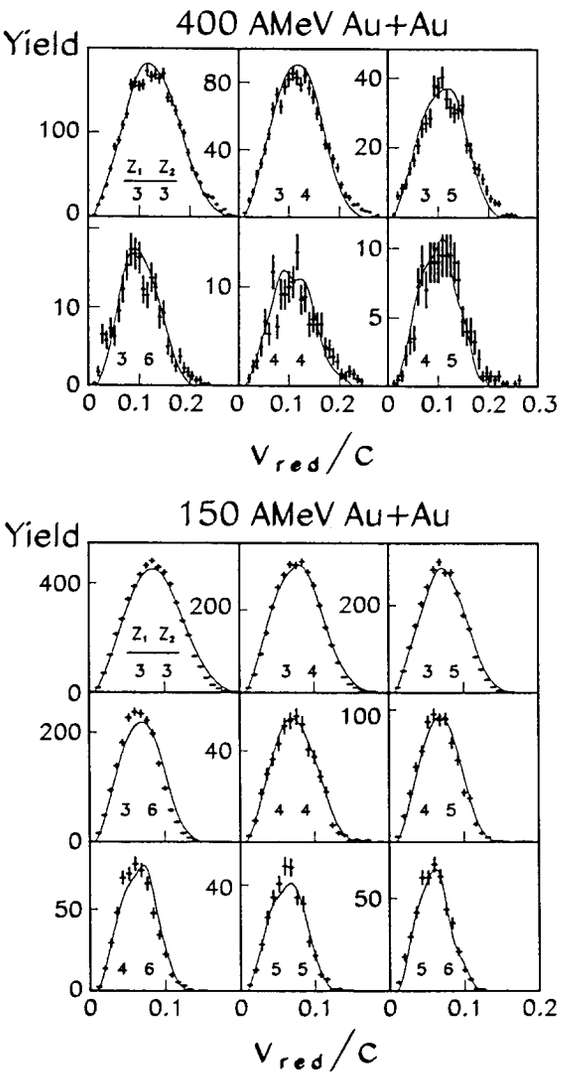
400 AMeV Au+Au
Yield
Z₁ Z₂
3 3
3 4
3 5
3 6
4 4
4 5
v_red/c
150 AMeV Au+Au
Yield
4 6
5 5
5 6
v_red/c

FIG. 2.

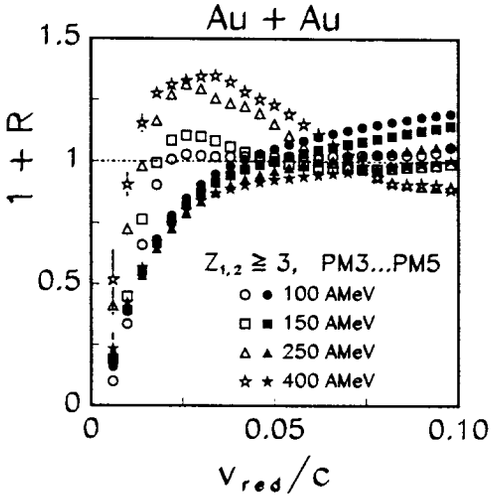

FIG. 3.

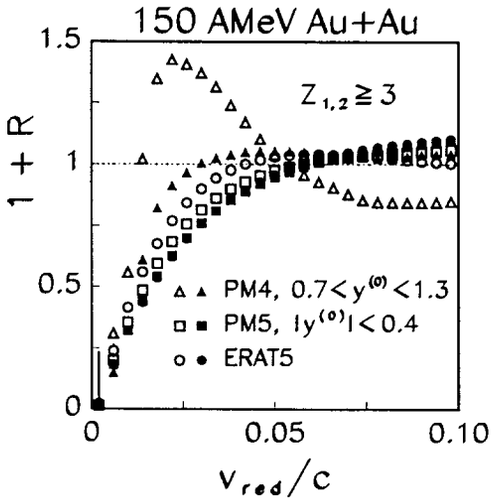

FIG. 4.

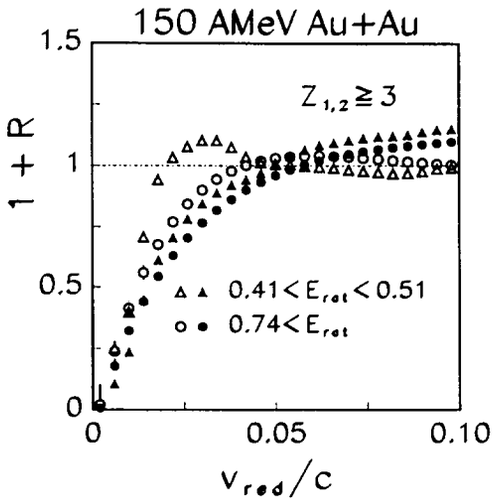

FIG. 5.

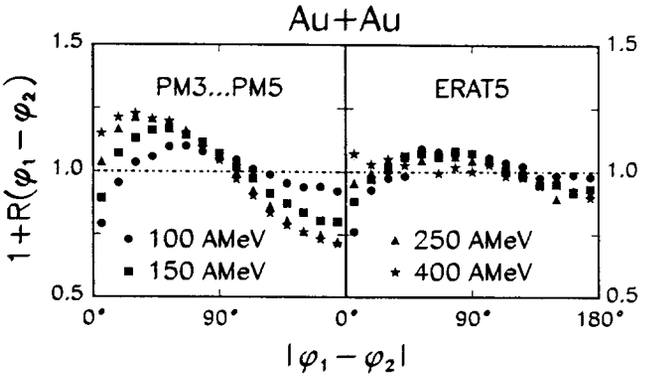
Au+Au
PM3...PM5
ERAT5
100 AMeV
150 AMeV
250 AMeV
400 AMeV
1+R(φ1 − φ2)
|φ1 − φ2|
1.5
1.0
0.5
0°
90°
180°

FIG. 6.

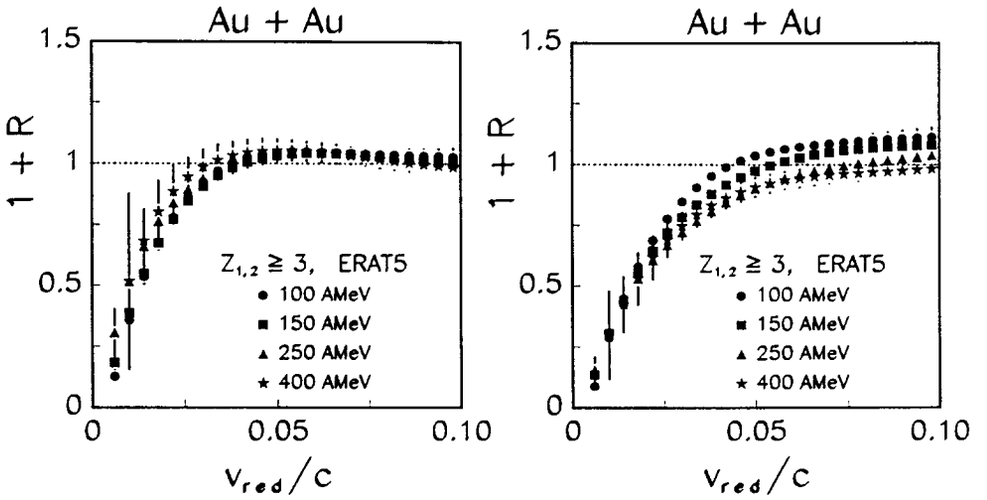
Au + Au
Au + Au
1 + R
Z1,2 ≥ 3, ERAT5
100 AMeV
150 AMeV
250 AMeV
400 AMeV
vred/c
1.5
1
0.5
0
0.05
0.10

FIG. 7.

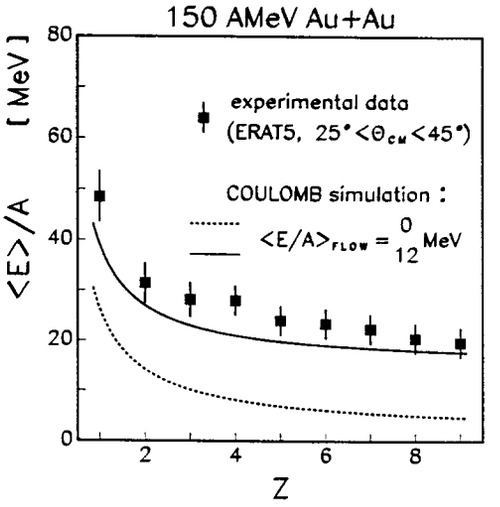
150 AMeV Au+Au
<E>/A [MeV]
experimental data
(ERAT5, 25°<Θcm<45°)
COULOMB simulation :
<E/A>FLOW = 0 / 12 MeV
Z

FIG. 8.

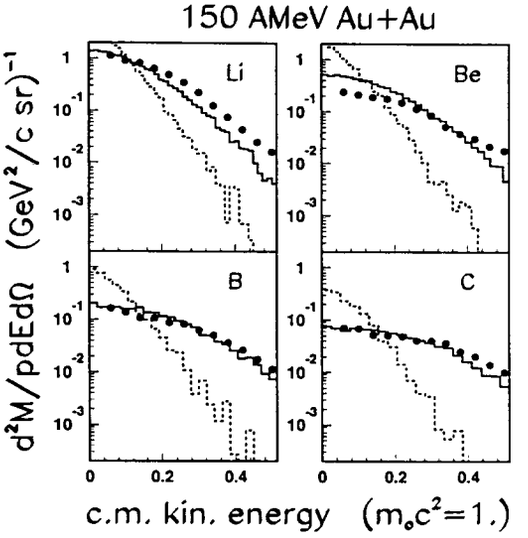
150 AMeV Au+Au
Li
Be
B
C
d²M/pdEdΩ (GeV²/c sr)⁻¹
c.m. kin. energy (m₀c²=1.)

FIG. 9.

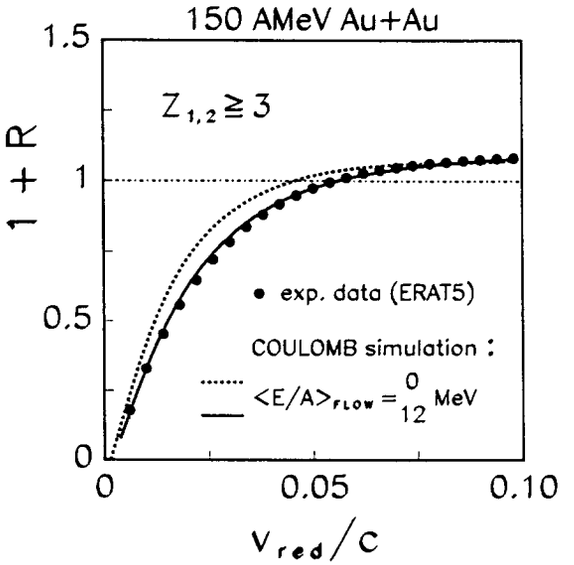
150 AMeV Au+Au
$Z_{1,2} \geq 3$
1 + R
1.5
1
0.5
0
0
0.05
0.10
v_{red}/c
• exp. data (ERAT5)
COULOMB simulation :
$<E/A>_{FLOW} = \begin{matrix}0\\12\end{matrix}$ MeV

FIG. 10.

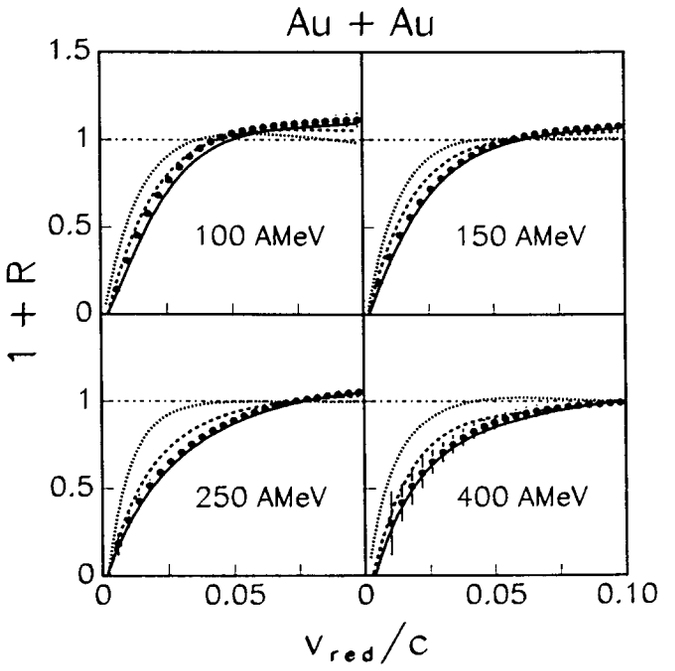
Au + Au
1 + R
1.5
1
0.5
0
100 AMeV
150 AMeV
250 AMeV
400 AMeV
0
0.05
0
0.05
0.10
v_{red}/c

FIG. 11.

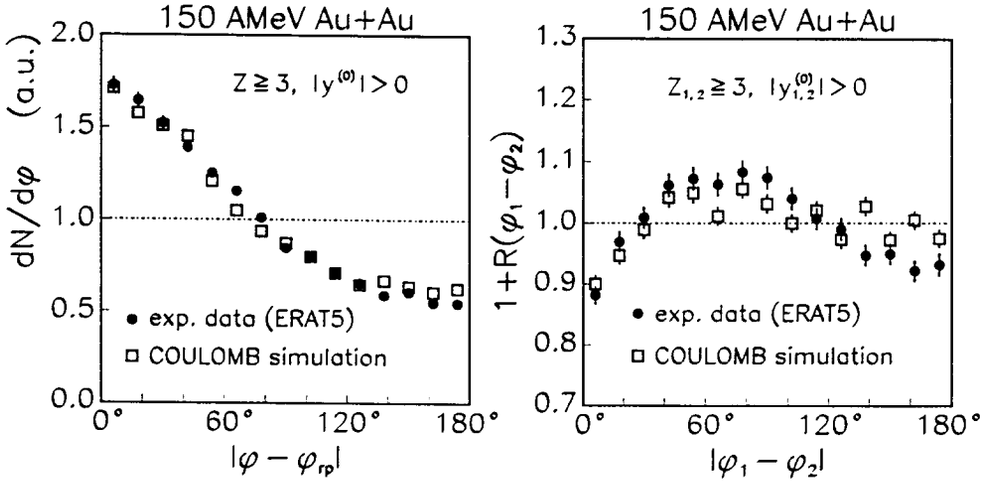

FIG. 12.

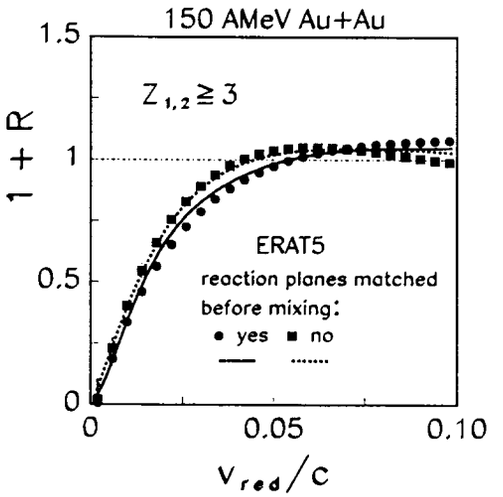

FIG. 13.

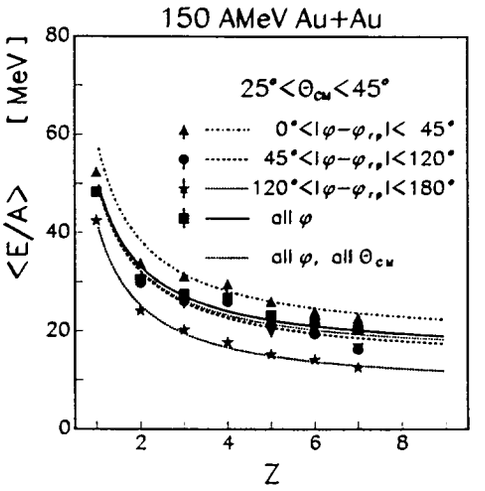

FIG. 14.